
Thermodynamic driving force of transient negative capacitance of ferroelectric capacitors

Yuanyuan Zhang, Xiaoqing Sun, Junshuai Chai, Hao Xu, Xueli Ma, Jinjuan Xiang, Kai Han, Xiaolei Wang, and Wenwu Wang*

Dr. Yuanyuan Zhang, Xiaoqing Sun, Junshuai Chai, Hao Xu, Prof. Xueli Ma, Jinjuan Xiang, Xiaolei Wang, Wenwu Wang

Key Laboratory of Microelectronics & Integrated Technology, Institute of Microelectronics, Chinese Academy of Sciences, and College of Microelectronics, University of Chinese Academy of Sciences, Beijing 100049, China

E-mail: wangxiaolei@ime.ac.cn

Prof. Kai Han

Department of Physics and Electronic Science, Weifang University, Weifang 261061, China

Keywords: Ferroelectric, negative capacitance, thermodynamic driving force

This paper investigates the thermodynamic driving force of transient negative capacitance (NC) in the series circuit of the resistor and ferroelectric capacitor (R -FEC). We find that the widely used Landau-Khalatnikov (L-K) theory, that is, the minimum of the Gibbs free energy, is inapplicable to explain the transient NC. The thermodynamic driving force of the transient NC phenomenon is the minimum of the difference between the elastic Gibbs free energy and the electric polarization work. The appearance of the transient NC phenomenon is not due to the widely accepted view that the ferroelectric polarization goes through the negative curvature region of elastic Gibbs free energy landscape (G_a). Instead, the transient NC phenomenon appears when the energy barrier of G_a disappears. The transient NC is dependent on both the intrinsic ferroelectric material parameters and extrinsic factors in the R -FEC circuit.

1. Introduction

Complementary metal-oxide-semiconductor field-effect transistor (MOSFET) technology¹ is the cornerstone of the contemporary information industry. Its ubiquity has been realized by the dramatic increase of its processing capacity every unit chip area², due to the exponential scaling of the MOSFET devices, well known as Moore's law. However, the supply voltage has not been proportionally reduced, and limited to ~0.8 V in modern integrated circuits, in order to effectively suppress the power consumption. The power consumption has been the bottleneck of scaling down the contemporary MOSFET devices³. The most effective way to reduce the power consumption of an integrated circuit is to reduce the supply voltage⁴⁻⁶. However, when the supply voltage is lowered, the drive current is sacrificed, which would decrease the operating speed of the transistor. The reason is that at least ~60 mV of gate voltage is needed to change the drain to source current by an order of magnitude, which is known as Boltzmann limit. In order to avoid this problem, it is necessary to have the highest possible on-off current ratio I_{ON}/I_{OFF} . This can be achieved by reducing the subthreshold swing (SS). For a classical MOSFET, the minimum SS is 60mV/decade at room temperature⁷, because of the Boltzmann distribution of channel carriers limit. To overcome this fundamental limit, the negative capacitance (NC) FETs⁸⁻²¹ have been proposed to amplify the semiconductor surface potential by the pioneering work of Salahuddin and Datta in 2008⁸. Moreover, the NC FETs are the most promising among the future steep subthreshold devices^{22, 23} since the discovery of ferroelectricity in doped hafnium oxide²⁴⁻³⁰.

So far there are two kinds of NC experimentally reported: (1) stabilized (steady-state) NC^{31, 32}, and (2) transient NC^{33, 34}. The stabilized NC has been experimentally demonstrated in FE-DE (ferroelectric-dielectric) heterostructures and superlattices of PZT/STO, BTO/STO, SRO/STO, SRO/GSO, and SRO/DSO by total capacitance enhancement³⁵⁻³⁷. Moreover, by forming polarization arrays of clockwise and anticlockwise vortex-like structures, the stabilized NC was also observed in epitaxial superlattices composed of ferroelectric PbTiO₃ and non-ferroelectric SrTiO₃³⁸. On the other hand, several models of steady-state NC have been proposed, associated with stabilizing the negative curvature region of ferroelectric double-well Gibbs energy landscape by adding the parabolic energy landscape of normal dielectric to the double-well landscape of ferroelectric³⁹. In addition, domain wall motion has been suggested to produce NC in a multidomain system⁴⁰⁻⁴³. Nevertheless, steady-state NC suffers from big disputes and doubts⁴⁴⁻⁴⁶. For the case of transient NC, it has been experimentally observed in a resistor-ferroelectric capacitor (*R*-FEC) network by applying a voltage pulse^{33, 42, 47-49}. The transient NC appears during the polarization switching of the ferroelectric material. Its physical origin is widely accepted as the mismatch between the free charges on the metal electrode and ferroelectric polarization^{46, 48, 50, 51}. So far, the understanding of the basic physics for transient NC is based on the Landau–Ginzburg–Devonshire (L-G-D) theory and the Landau-Khalatnikov (L-K) equation⁵²⁻⁵⁵. The polarization state in this theory is described by double-well Gibbs free energy landscape as a function of the polarization P , where there exist two stable polarization states with the minimum

energy. When a voltage pulse is applied to the ferroelectric capacitor, the polarization state will switch along the direction of Gibbs free energy minimization⁵⁵. It is worth noting that this process is only valid under the electric field $E=\text{constant}$ across the ferroelectric capacitor. However, E is not a constant field but changes with time in transient NC^{46, 56, 57}, which will be shown in section 2. This means that the conventional L-K theory is improper to explain the transient NC phenomenon. Thus, it is necessary to reconsider the physical origin and find the thermodynamic driving force for the transient NC phenomenon. Moreover, the modern explanation of transient NC lacks a detailed physical picture, and a thorough understanding of the underlying physics is still absent. The above issues need urgent understanding because it limits NC progress and is critical for guiding the design of device structure such as ferroelectric parameters.

In this work, we revisit the thermodynamic driving force of the transient NC phenomenon in the R -FEC circuit. We find that the thermodynamic driving force is the minimization of a new thermodynamic function η instead of Gibbs free energy G , where η is equal to the difference between the elastic Gibbs free energy and the electric polarization work. This means that the polarization switches along the direction of η minimization. Moreover, this viewpoint is further supported by the analysis based on experimental P - E curves. In addition, we also find that the appearance of the transient NC phenomenon is not due to the widely accepted viewpoint that the ferroelectric polarization goes through the negative curvature region of elastic Gibbs free energy landscape (G_a). Instead, the NC phenomenon

appears when the energy barrier of G_a disappears. Moreover, the transient NC is dependent on both the intrinsic ferroelectric material parameters and extrinsic factors in the R -FEC circuit.

2. Limits of Landau-Khalatnikov (L-K) equation in explaining the transient NC

Generally, transient NC is explained by the L-K equation. The L-K equation, describes a thermodynamics process, where the FE polarization obeys the Gibbs free energy minimization, can be expressed as

$$\rho \frac{dP}{dt} = - \frac{\partial G}{\partial P} \quad (1)$$

where ρ is the viscosity coefficient which means the delay of polarization P with respect to the electric field. G is Gibbs free energy, which can be expanded in terms of P based on L-G-D theory, expressed as⁵⁸

$$G = \alpha P^2 + \beta P^4 + \gamma P^6 - PE = G_a - PE \quad (2)$$

where α , β , and γ are the thermodynamic expansion coefficients, E is the electric field across the FE capacitor, and G_a is elastic Gibbs free energy. In L-K equation, the term dG/dP can be regarded as driving force F which causes polarization switching toward the local minimum of the free energy. The traditional expression of F is

$$F = - \frac{\partial G}{\partial P} = E - 2\alpha P + 4\beta P^3 + 6\gamma P^5 = E - \frac{dG_a}{dP} \quad (3)$$

The above theory is widely used to explain the transient NC^{42, 47}, and successfully in line with the experimental results^{42, 47}. It should be noted that the key of the L-K equation in explaining the transient NC is the minimization of the Gibbs free energy G . However, there is a precondition of using the G minimization, that is, isoelectric

field, which has been ignored during the previous application of the L-K equation in understanding the transient NC. Here we show why the isoelectric field is the precondition. According to the first and second laws of thermodynamics, we have $TdS \geq dU - dW$, where T , S , and U are the temperature, the entropy, and the total internal energy of the system, respectively, and W is the external work. In FE materials, the total differential of external work can be expressed as $dW = Xdx + EdD$, where Xdx and EdD are mechanic work and electric work, respectively. x is the elastic strain, X is the stress and D is the electric displacement field. Thus, the total differential of internal energy can be given as $dU \leq TdS + Xdx + EdP + d(1/2\varepsilon_0 E^2)$. Changing the order of the last equation, it can be rewritten as

$$d(U - \frac{1}{2}\varepsilon_0 E^2) - TdS - Xdx - EdP \leq 0. \quad (4)$$

In the process of isothermal ($dT=0$) and without any stress ($dX=0$), Equation (4) is further written as

$$d(U - \frac{1}{2}\varepsilon_0 E^2) - TdS - SdT - Xdx - x dX - EdP \leq 0$$

or

$$d(U - TS - Xx - \frac{1}{2}\varepsilon_0 E^2) - EdP \leq 0. \quad (5)$$

We consider the case of assuming $E = \text{constant}$. Correspondingly, $PdE=0$. Adding this item to the left side of the Equation (5) obtains

$$d(U - TS - Xx - EP - \frac{1}{2}\varepsilon_0 E^2) \leq 0. \quad (6)$$

Here, the items $(U - TS - Xx - EP - 1/2\varepsilon_0 E^2)$ in brackets is Gibbs free energy G . Then, Equation (6) becomes

$$dG \leq 0. \quad (7)$$

This indicates that the Gibbs free energy no longer increases at constant electric fields. Thus, the polarization switching along the direction of Gibbs free energy minimization is only applicable when keeping the electric field across FE constant. The next question is whether the transient NC process meets the isoelectric field condition. From the reported experimental P - E curves of transient NC measured on positive rectangular voltage pulse in the R -FEC circuit^{42, 47}, as shown in Figures 2(a) and 2(b), we can find that the electric field across the ferroelectric is changed with polarization during the transient NC process, rather than a constant. Moreover, based on these experimental results, we calculate the corresponding Gibbs free energy landscape G as a function of polarization P , as shown in Figures 2 (c) and 2(d). It shows that as P increases, G first increases and then decreases. This indicates that the system will settle P in such a way that does not minimize the G . Consequently, the L-K theory, that is, G minimization is not applicable in explaining the transient NC. It is necessary to reconsider the thermodynamic process of FE polarization during transient NC.

3. Thermodynamic driving force of transient NC

The thermodynamics driving force of transient NC is investigated. Based on the above discussion, we consider the case of $E \neq \text{constant}$. We come back to Equation (5), which is still applicable for the case $E \neq \text{constant}$. According to Equation (5), elastic Gibbs free energy G_a is given by^{59, 60}

$$\begin{aligned}
G_a &= U - TS - Xx - \frac{1}{2}\epsilon_0 E^2 \\
&= \alpha P^2 + \beta P^4 + \gamma P^6
\end{aligned} \tag{8}$$

Then, Equation (5) can be rewritten as $dG_a - EdP \leq 0$. Here we define a new thermal potential η that satisfies

$$d\eta = dG_a - EdP \leq 0. \tag{9}$$

This means that the essence of transient NC follows the minimization of the new thermal potential η . Taking an integration of the above equation yields

$$\int_{\eta_0}^{\eta} d\eta = \int_{G_{a0}}^{G_a} dG' - \int_{P_0}^P EdP \leq 0$$

or

$$\eta = G_a - \int_{P_0}^P EdP + (\eta_0 - G_{a0}) \tag{10}$$

where η_0 and G_{a0} express η and G_a at the initial state, respectively. Equation (10) indicates that the new thermal potential η is equal to the difference between the elastic Gibbs free energy and electric polarization work. Thus the ferroelectric polarization changes toward the direction where the thermal potential η decreases, and this can be equally expressed by

$$\rho \frac{dP}{dt} = - \frac{\partial \eta}{\partial P}. \tag{11}$$

Taking Equation (10) into Equation (11) gets

$$\rho \frac{dP}{dt} = - \frac{\partial \eta}{\partial P} = E - \frac{dG_a}{dP}. \tag{12}$$

Combining with Equation (1), we find an interesting result, that is, the expression of $\partial \eta / \partial P$ and $\partial G / \partial P$ is the same. However, thermal potential η and G are essentially different because they have completely different physical meanings. Based on the experimental P - E curves [see Fig.2(a) and (b)], we calculate the thermal potential η ,

as shown in Figures 2(c) and (d). It shows that the η exhibits a monotonous decreasing trend. Thus the system will settle P in such a way that minimizes η instead of G , that is, the thermodynamic driving force of transient NC is the minimization of the η instead of G .

From Equations (1) and (12), the partial derivative of the Gibbs free energy G with respect to P for a given V_{FE} (or E) is equal to the derivative of η with respect to the P , that is, $d\eta/dP = \partial G/\partial P|_{E=\text{constant}}$. This indicates that at a given state (knowing P and E or V_{FE}), the polarization switching direction can be judged by the way of minimizing G . This means that we could use the Gibbs free energy landscape at a given E to predict the polarization switching direction of the ferroelectric.

4. Transient behavior of NC

The dynamic process of polarization switching in the R -FEC circuit is further investigated by using numerical simulations. Figure 3 shows the simulated FE voltage response of the R -FEC circuit under an applied voltage pulse (-3 V \rightarrow 3 V), based on the Equation (12). The simulation parameters²⁵ are listed in Table 1. In Figure 3, the states 1 and 18 represent the initial and final stable states, and the states 2~17 express the unstable states. Along the transient polarization states 1 \rightarrow 2 \rightarrow 3 \rightarrow ... \rightarrow 16 \rightarrow 17 \rightarrow 18, the ferroelectric voltage V_{FE} and ferroelectric polarization P change with time, where the polarization continues to increase, while the ferroelectric voltage increases initially, then decreases, and finally increases again. It can be seen that the NC region appears from state 7 to 12, where $dE/dP < 0$.

In order to understand the fundamental physics of the transient NC, we further calculate the Gibbs free energy G landscape as a function of P at different FE voltages, as shown in Figure 4. The G curve is dependent on the electric field across the ferroelectric, and changes as the ferroelectric state changes. Here we define the polarization corresponding to the localized minimum of G as P_{min} , which are shown as the black square dots in Figure 4. For the process of states $1 \rightarrow 2 \rightarrow 3 \rightarrow 4 \rightarrow 5$ (V_{FE} : $-3 \rightarrow -1.56 \rightarrow -1 \rightarrow 0 \rightarrow +1$ V), the transient FE polarization state at each ferroelectric voltage is always located on the left side of P_{min} . Thus the polarization at these states increases. For the state 6 ($V_{FE} = +1.75$ V), there are two zero derivative points in the corresponding G curve. One zero derivative point corresponding to negative polarization is not an extreme point (here denoted as P_{nonmin}), which means that the energy barrier disappears. At this state, the polarization is localized on the left side of the P_{nonmin} , and consequently, the polarization still increases. For the state 7 ($V_{FE} = +1.79$ V), there is only one zero derivative points, i.e., P_{min} , localized at the positive polarization region in the corresponding G curve, as shown in Figure 4. Moreover, there is no energy barrier, and the polarization increases toward P_{min} . For the state 8, the G curve is the same as that of case 6. However, the polarization state has been localized on the right side of the P_{nonmin} . Thus, for the process of states $6 \rightarrow 7 \rightarrow 8$ (V_{FE} : $+1.75 \rightarrow +1.79 \rightarrow +1.75$ V), the G curve corresponding to each state shows a monotonous decreasing trend and has only one minimum point, which is localized in the positive polarization region (~ 0.17 C/cm²). These results indicate that the polarization continues to increase. For the process states $9 \rightarrow 10 \rightarrow 11 \rightarrow 12$ (V_{FE} :

+1→0→-1→-1.56 V), the G curve has the double-well energy landscape, i.e., the energy barrier has appeared. However, the transient polarization state has been always on the right side of the maximum point of the G curve at the corresponding ferroelectric voltage. This means that the transient polarization state has rolled over the energy barrier of the G curve, and the polarization increases toward the right P_{\min} . This leads to an interesting phenomenon that the polarization for states 7~12 further increases as the voltage decreases, which indicates that the NC phenomenon appears in this process. The process of states 13~18 is similar to states 1~5, that is, the transient polarization state at each ferroelectric voltage is always located on the left side of P_{\min} , and the polarization increases with the increase of ferroelectric voltage.

The black line in Figure 4 gives the Gibbs free energy during the whole transient NC process. It can be seen that the G is not always decreasing, but changes like an ‘M’ shape. Above dynamic process reveals that the trend of transient polarization obeys the Gibbs free energy minimization rule under a fixed voltage. However, the whole dynamic process of polarization switching from states 1~18 doesn't satisfy the Gibbs free energy minimization because the voltage is a variable and changed during the transient NC process.

Actually, above dynamic process follows the η minimization rule. Figure 5 shows the G and η during the transient NC process. The G initially increases, then decreases, then increases, and finally decreases. Thus the G does not always decrease, as expected by the L-K theory. On the other hand, the η always decreases. This further

confirms our opinion, that is, the thermodynamic driving force of transient NC is indeed the minimization of η rather than G .

5. Physical origin of transient NC appearance

We discuss the fundamental physics of transient NC. Figure 6(a) shows the ideal P - E curve obtained by differentiating G_a with respect to P . The ideal P - E curve is also well known as the ‘S’ shape curve. Also shown in Figure 6(a) is the real P - E curve of transient NC. For each P , the $\partial G_a / \partial P$ is equal to E of the ideal P - E curve (here denoted as E_0). From Equation (12), we can get that the dP/dt is proportional to the $E_r - E_0$, where E_r represents the E of transient NC (ideal P - E curve). Moreover, the $E_r - E_0$ is equal to $-\partial G / \partial P$, which reflect the negative slope of the G vs. P curve. The corresponding $E_r - E_0$ profile as a function of P (difference between the black and red lines for each P) is given in Fig6(b).

Here we divide the real P - E curve into five regions, as shown in Figure 6(a). When $E=E_1$, the energy barrier of the corresponding G curve just disappeared, as shown in Figure 6(c). For region I, the G landscape is schematically shown in Figure 6(d). There is only one extreme point, here minimum, and denoted as P_{\min} . There is no energy barrier, i.e., local maximum. The real P is always localized on the left side of the P_{\min} . Moreover, the change rate of P (dP/dt) corresponds to the slope of the G curve, based on Equation (12). And the dP/dt is less than the (dQ/dt) , here the Q is the free charges on the metal plate. Thus the dV_{FE}/dt is positive, and the V_{FE} increases. For region II, the G landscape is schematically shown in Figure 6(e). There are three extreme points, i.e., two local minimum points ($P_{\min, L}$ and $P_{\min, R}$) and one local

maximum point (P_{\max}). The barrier appears. The real P is always localized on the left side of the $P_{\min, L}$. Moreover, the dP/dt is less than the (dQ/dt) . Thus the dV_{FE}/dt is positive, and the V_{FE} increases. For region III (state $a \rightarrow b \rightarrow c$), the G landscape is schematically shown in Figure 6(f). There is only one extreme point (P_{\min}). The barrier disappears. The real P increases toward the P_{\min} . From state a to b [see Figure 6(a)], there is no NC phenomenon. From the state b to c , the NC phenomenon appears. The dP/dt is increasing and becomes larger than dQ/dt from state b . This is attributed to that the slope of G curve becomes steep from state b to c [see Figure 6(b)]. An interesting phenomenon is that the dP/dt before the NC appearance (e.g., $a \rightarrow b$) is larger than that of state b . This means that the NC is not only dependent on the dP/dt . For region IV (state $c \rightarrow d \rightarrow e$), the G landscape is schematically shown in Figure 6(g). There are three extreme points, i.e., two local minimum points ($P_{\min, L}$ and $P_{\min, R}$) and one local maximum point (P_{\max}). The barrier appears. However, the polarization P has rolled over the barrier and quickly increases toward the right $P_{\min, R}$. The slope of the G curve in this region is large, especially for the region of state c to d . In other words, the distance between the black real P - E line and the red ideal P - E line is large. This results in larger dP/dt than the (dQ/dt) , and consequently NC phenomenon. From the state d , the G curve begins to flatten. The dQ/dt catches up with the dP/dt again, leading to that the NC phenomenon disappears. For region V (state $e \rightarrow f \rightarrow g$), the G landscape is schematically shown in Figure 6(h). There is only one extreme point, similar to region III [see Figure 6(f)]. The G curve in this region keeps flat and there is still no NC phenomenon. From the above discussion, it can be concluded that the

NC appears when the barrier disappears (region $b \rightarrow c$) or the polarization state has rolled over the barrier (region $c \rightarrow d$). There is no case that the polarization climbs up to the barrier top. In addition, the elastic Gibbs free energy G_a profile is shown in Figure 6(i). The polarization states $a \rightarrow b \rightarrow \dots \rightarrow g$ are also shown. It should be noted that the negative curvature region of G_a is different from the real transient NC region, indicating that the transient NC cannot be judged by the negative curvature of G_a .

Based on Equations. (11) and (12), $\partial V_{FE}/\partial t$, at a given time t_0 , can be expressed as

$$\begin{aligned}
 \left. \frac{\partial V_{FE}}{\partial t} \right|_{t=t_0} &= \frac{d_{FE}}{\varepsilon_0} \left(\left. \frac{\partial Q}{\partial t} \right|_{t=t_0} - \left. \frac{\partial P}{\partial t} \right|_{t=t_0} \right) \\
 &= \frac{d_{FE}}{\varepsilon_0} \left(\frac{V_s - V_{FE_0}}{R} + \left. \frac{\partial G_a}{\rho \partial P} \right|_{t=t_0} - E_0 \right) \\
 &= \frac{d_{FE}}{\varepsilon_0} \left(\frac{V_s}{R} + \frac{2\alpha P_0 + 4\beta P_0^3 + 6\gamma P_0^5}{\rho} - \left(1 + \frac{d_{FE}}{R} \right) E_0 \right)
 \end{aligned} \tag{13}$$

where P_0 and E_0 are the polarization and electric field across the ferroelectric at a given time t_0 , respectively. d_{FE} is the ferroelectric physical thickness. This equation suggests that the appearance of NC is not only related to V_s , R , P_0 and E_0 , but also related to α , β , γ and ρ . And these four parameters are related to the ferroelectric material characteristics (intrinsic), while the V_s and R are related to the extrinsic characteristics of the R -FEC circuit. This means that the appearance of NC is not only dependent on the ferroelectric material itself but dependent on some extrinsic factors. By further adjusting the value of α , β , and γ , it is possible to realize that the change of polarization with time is greater than the free charge change with time, leading to the appearance of NC.

In addition, we also explore a physical criterion for transient NC. In the *R*-FEC circuit, electrostatic force work of ferroelectric polarization is given as $W=\int E dP$, and then second-order differentiating W with respect to P is $d^2W/dP^2=dE/dP$. Since $dE/dP<0$ is required for the transient NC, W should satisfy $d^2W/dP^2<0$, which means that the negative curvature of electrostatic force work is a criterion for transient NC. This is obviously different from the traditional criterion that the transient NC region appears in the portion of the negative curvature of elastic Gibbs free energy G_a ($d^2G_a/dP^2<0$). In order to verify these two criteria, we differentiate $G_a(W)$ with respect to P and obtain the 'S' shaped (transient) P - E curves, as shown in Figure 7. It is found that the transient polarization states in Figure 7 can be directly mapped on the transient P - E curve, but not on the 'S' curve. This indicates that the transient NC can indeed be judged by the negative curvature of electrostatic force work instead of elastic Gibbs free energy.

4. Conclusion

In conclusion, using the Landau-Ginzburg-Devonshire (L-G-D) theory and the first and second laws of thermodynamics, we have detailedly studied the thermodynamic process of transient NC in the *R*-FEC circuit. Our results show that the dynamic process of polarization switching for transient NC follows the minimization of the new thermodynamic potential η (the difference between the elastic Gibbs free energy and the electric polarization work). The conventional view that the Gibbs free energy minimization is not applicable. Furthermore, this viewpoint is verified by the analysis

based on experimental P - E curves and numerical simulation of the dynamic process of polarization switching for transient NC. In addition, the appearance of the transient NC phenomenon is not due to the widely accepted view that the ferroelectric polarization goes through the negative curvature region of elastic Gibbs free energy landscape (G_a). Instead, the transient NC phenomenon appears when the G_a energy barrier disappears. Moreover, the transient NC is dependent on both the intrinsic ferroelectric material parameters and extrinsic factors in the R -FEC circuit. The work provides a comprehensive explanation for the dynamic process of transient NC.

Acknowledgments

This work is supported in part by the National Key Project of Science and Technology of China (Grant no. 2017ZX02315001-002).

Received: ((will be filled in by the editorial staff))

Revised: ((will be filled in by the editorial staff))

Published online: ((will be filled in by the editorial staff))

References

1. Mistry, K. et al. A 45nm logic technology with high- k metal gate transistors, strained silicon, 9 Cu interconnect layers, 193nm dry patterning, and 100% Pb-free packaging. In *2007 IEEE International Electron Devices Meeting (IEDM)* 247-250. (IEEE, 2007).
2. Laws, D. 13 sextillion & counting: the long & winding road to the most frequently manufactured human artifact in history. *CHM Blog* (2018).
3. Hoffmann, M., Slesazeck, S., Schroeder, U. & Mikolajick, T. What's next for negative capacitance electronics? *Nat. Electron.* 504-506 (2020).

-
4. Hoffmann, M., Pešić, M., Slesazeck, S., Schroeder, U. & Mikolajick, T. On the stabilization of ferroelectric negative capacitance in nanoscale devices. *Nanoscale* **10**, 10891-10899 (2018).
 5. Park, H. W., Roh, J., Lee, Y. B. & Hwang, C. S. Modeling of negative capacitance in ferroelectric thin films. *Adv. Mater.* **31**, 1805266 (2019).
 6. Theis, T. N. & Solomon, P. M. It's time to reinvent the transistor! *Science* **327**, 1600-1601 (2010).
 7. Zhirnov, V. V. & Cavin, R. K. Nanoelectronics: Negative capacitance to the rescue? *Nat. Nanotechnol* **3**, 77 (2008).
 8. Salahuddin, S. & Dattat, S. Use of negative capacitance to provide voltage amplification for low power nanoscale devices. *Nano Lett.* **8**, 405-410 (2008).
 9. Dubourdieu, C. et al. Switching of ferroelectric polarization in epitaxial BaTiO₃ films on silicon without a conducting bottom electrode. *Nat. Nanotechnol* **8**, 748-754 (2013).
 10. Jain, A. & Alam, M. A. Stability constraints define the minimum subthreshold swing of a negative capacitance field-effect transistor. *IEEE Trans. Electron Devices* **61**, 2235-2242 (2014).
 11. Wang, X. et al. Ultrasensitive and broadband MoS₂ photodetector driven by ferroelectrics. *Adv. Mater.* **27**, 6575-6581 (2015).
 12. Salvatore, G. A., Bouvet, D. & Ionescu, A. M. Demonstration of subthreshold swing smaller than 60mV/decade in Fe-FET with P(VDF-TrFE)/SiO₂ gate stack. In *2008 IEEE International Electron Devices Meeting (IEDM)* 1-4.

-
- (IEEE, 2008).
13. Cheng, C. H. & Chin, A. Low-Voltage Steep Turn-On pMOSFET Using Ferroelectric High-k Gate Dielectric. *IEEE Electron Device Lett.* **35**, 274-276 (2014).
 14. Lee, M.-H. et al. Prospects for ferroelectric HfZrO_x FETs with experimentally CET = 0.98 nm, SS_{for} = 42 mV/dec, SS_{rev} = 28 mV/dec, switch-off < 0.2 V, and hysteresis-free strategies. In *2015 IEEE International Electron Devices Meeting (IEDM)* 22.25. 21-22.25. 24. (IEEE, 2015).
 15. Li, K.-S. et al. Sub-60mV-swing negative-capacitance FinFET without hysteresis. In *2015 IEEE International Electron Devices Meeting (IEDM)* 22.26. 21-22.26. 24. (IEEE, 2015).
 16. Zhou, J. et al. Ferroelectric HfZrO_x Ge and GeSn PMOSFETs with sub-60 mV/decade subthreshold swing, negligible hysteresis, and improved I_{DS}. In *2016 IEEE International Electron Devices Meeting (IEDM)* 12.12. 11-12.12. 14. (IEEE, 2016).
 17. McGuire, F. A., Cheng, Z., Price, K. & Franklin, A. D. Sub-60 mV/decade switching in 2D negative capacitance field-effect transistors with integrated ferroelectric polymer. *Appl. Phys. Lett.* **109**, 093101 (2016).
 18. Lee, M. et al. Extremely Steep Switch of Negative-Capacitance Nanosheet GAA-FETs and FinFETs. In *2018 IEEE International Electron Devices Meeting (IEDM)* 31.38. 31-31.38. 34. (IEEE, 2018).
 19. Si, M. et al. Steep-slope hysteresis-free negative capacitance MoS₂ transistors.

-
- Nat. Nanotechnol* **13**, 24-28 (2018).
20. Alam, M. A., Si, M. & Ye, P. D. A critical review of recent progress on negative capacitance field-effect transistors. *Appl. Phys. Lett.* **114**, 090401 (2019).
 21. Cao, W. & Banerjee, K. Is negative capacitance FET a steep-slope logic switch? *Nat. Comm.* **11**, 196 (2020).
 22. Kwon, D. et al. Improved subthreshold swing and short channel effect in FDSOI n-channel negative capacitance field effect transistors. *IEEE Electron Device Lett.* **39**, 300-303 (2017).
 23. Kwon, D. et al. Negative capacitance FET with 1.8-nm-thick Zr-doped HfO₂ oxide. *IEEE Electron Device Lett.* **40**, 993-996 (2019).
 24. Böске, T., Müller, J., Bräuhäus, D., Schröder, U. & Bätger, U. Ferroelectricity in hafnium oxide thin films. *Appl. Phys. Lett.* **99**, 102903 (2011).
 25. Müller, J. et al. Ferroelectric Zr_{0.5}Hf_{0.5}O₂ thin films for nonvolatile memory applications. *Appl. Phys. Lett.* **99**, 112901 (2011).
 26. Dünkel, S. et al. A FeFET based super-low-power ultra-fast embedded NVM technology for 22nm FDSOI and beyond. In *2017 IEEE International Electron Devices Meeting (IEDM)* 19.17. 11-19.17. 14. (IEEE, 2017).
 27. Kim, K. D. et al. Transient Negative Capacitance Effect in Atomic - Layer - Deposited Al₂O₃/Hf_{0.3}Zr_{0.7}O₂ Bilayer Thin Film. *Adv. Funct. Mater.* **29**, 1808228 (2019).

-
28. Shimizu, T. et al. The demonstration of significant ferroelectricity in epitaxial Y-doped HfO₂ film. *Sci. Rep.* **6**, 32931 (2016).
 29. Hoffmann, M. et al. Negative Capacitance for Electrostatic Supercapacitors. *Adv. Energy Mater.* **9**, 1901154 (2019).
 30. Tian, X. et al. Evolution of ferroelectric HfO₂ in ultrathin region down to 3 nm. *Appl. Phys. Lett.* **112**, 102902 (2018).
 31. Muller, J. et al. Ferroelectricity in simple binary ZrO₂ and HfO₂. *Nano Lett.* **12**, 4318-4323 (2012).
 32. Zubko, P. et al. Negative capacitance in multidomain ferroelectric superlattices. *Nature* **534**, 524-528 (2016).
 33. Khan, A. I. et al. Negative capacitance in a ferroelectric capacitor. *Nat. Mater.* **14**, 182-186 (2015).
 34. Jin, C., Saraya, T., Hiramoto, T. & Kobayashi, M. Transient Negative Capacitance as Cause of Reverse Drain-induced Barrier Lowering and Negative Differential Resistance in Ferroelectric FETs. In *2019 Symposium on VLSI Technology* T220-T221. (IEEE, 2019).
 35. Khan, A. I. et al. Experimental evidence of ferroelectric negative capacitance in nanoscale heterostructures. *Appl. Phys. Lett.* **99**, 113501 (2011).
 36. Appleby, D. J. et al. Experimental observation of negative capacitance in ferroelectrics at room temperature. *Nano Lett.* **14**, 3864-3868 (2014).

-
37. Gao, W. et al. Room-temperature negative capacitance in a ferroelectric–dielectric superlattice heterostructure. *Nano Lett.* **14**, 5814-5819 (2014).
 38. Yadav, A. K. et al. Spatially resolved steady-state negative capacitance. *Nature* **565**, 468-471 (2019).
 39. Kobayashi, M., Jang, K., Ueyama, N. & Hiramoto, T. Negative capacitance as a performance booster for tunnel FET. In *2016 IEEE Silicon Nanoelectronics Workshop (SNW)* 150-151. (IEEE, 2016).
 40. Luk'yanchuk, I., Sene, A. & Vinokur, V. M. Electrodynamics of ferroelectric films with negative capacitance. *Phys. Rev. B* **98**, (2018).
 41. Luk'yanchuk, I., Tikhonov, Y., Sene, A., Razumnaya, A. & Vinokur, V. M. Harnessing ferroelectric domains for negative capacitance. *Communications Physics* **2**, 22 (2019).
 42. Hoffmann, M. et al. Direct observation of negative capacitance in polycrystalline ferroelectric HfO₂. *Adv. Funct. Mater.* **26**, 8643-8649 (2016).
 43. Íñiguez, J., Zubko, P., Luk'yanchuk, I. & Cano, A. Ferroelectric negative capacitance. *Nat. Rev. Mater.* **4**, 243-256 (2019).
 44. Liu, Z., Bhuiyan, M. & Ma, T. A critical examination of 'quasi-static negative capacitance'(QSNC) theory. In *2018 IEEE International Electron Devices Meeting (IEDM)* 31.32. 31-31.32. 34. (IEEE, 2018).
 45. Van Houdt, J. & Roussel, P. Physical model for the steep subthreshold slope in ferroelectric FETs. *IEEE Electron Device Lett.* **39**, 877-880 (2018).

-
46. Kittl, J. et al. On the validity and applicability of models of negative capacitance and implications for MOS applications. *Appl. Phys. Lett.* **113**, 042904 (2018).
 47. Kobayashi, M., Ueyama, N., Jang, K. & Hiramoto, T. Experimental study on polarization-limited operation speed of negative capacitance FET with ferroelectric HfO₂. In *2016 IEEE International Electron Devices Meeting (IEDM)* 12.13. 11-12.13. 14. (IEEE, 2016).
 48. Kim, Y. J. et al. Voltage Drop in a Ferroelectric Single Layer Capacitor by Retarded Domain Nucleation. *Nano Lett.* **17**, 7796-7802 (2017).
 49. Sharma, P., Zhang, J., Ni, K. & Datta, S. Time-Resolved Measurement of Negative Capacitance. *IEEE Electron Device Lett.* **39**, 272-275 (2018).
 50. Song, S. J. et al. Alternative interpretations for decreasing voltage with increasing charge in ferroelectric capacitors. *Sci. Rep.* **6**, (2016).
 51. Saha, A. K., Datta, S. & Gupta, S. K. “Negative capacitance” in resistor-ferroelectric and ferroelectric-dielectric networks: Apparent or intrinsic? *J. Appl. Phys.* **123**, 105102 (2018).
 52. Landau, L. D. & Lifshitz, E. M. *Electrodynamics of Continuous Media* (Pergamon, Oxford, 1960).
 53. Ginzburg, V. On the dielectric properties of ferroelectric (segnette-electric) crystals and barium titanate. *Zh. Eksp. Teor. Fiz* **15**, 739-749 (1945).
 54. Devonshire, A. F. Theory of barium titanate: Part I. *Phil. Mag.* **40**, 1040-1063 (1949).

-
55. Landau, L. D. On the theory of phase transitions. I. *Zh. Eksp. Teor. Fiz.* **11**, 19 (1937).
 56. Majumdar, K., Datta, S. & Rao, S. P. Revisiting the Theory of Ferroelectric Negative Capacitance. *IEEE Trans. Electron Devices* **63**, 2043-2049 (2016).
 57. Chang, S.-C., Avci, U. E., Nikonov, D. E., Manipatruni, S. & Young, I. A. Physical origin of transient negative capacitance in a ferroelectric capacitor. *Phys. Rev. Appl.* **9**, 014010 (2018).
 58. Chang, S.-C., Avci, U. E., Nikonov, D. E. & Young, I. A. A thermodynamic perspective of negative-capacitance field-effect transistors. *IEEE J. Explor. Solid-State Comput. Devices Circuits* **3**, 56-64 (2017).
 59. Ricinschi, D. et al. Analysis of ferroelectric switching in finite media as a Landau-type phase transition. *J. Phys. Condens. Matter* **10**, 477-492 (1998).
 60. Hoffmann, M. et al. Unveiling the double-well energy landscape in a ferroelectric layer. *Nature* **565**, 464-467 (2019).

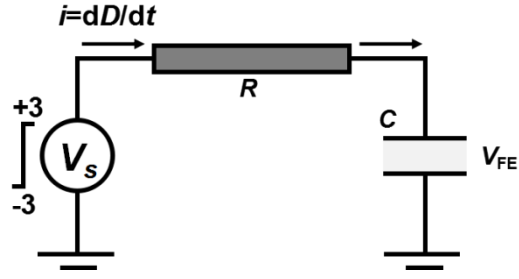


Figure 1. The schematic of an R -FEC circuit. C denotes the FE capacitor and R represents the external resistor. V and V_s are the voltage across the FE and the applied voltage, respectively.

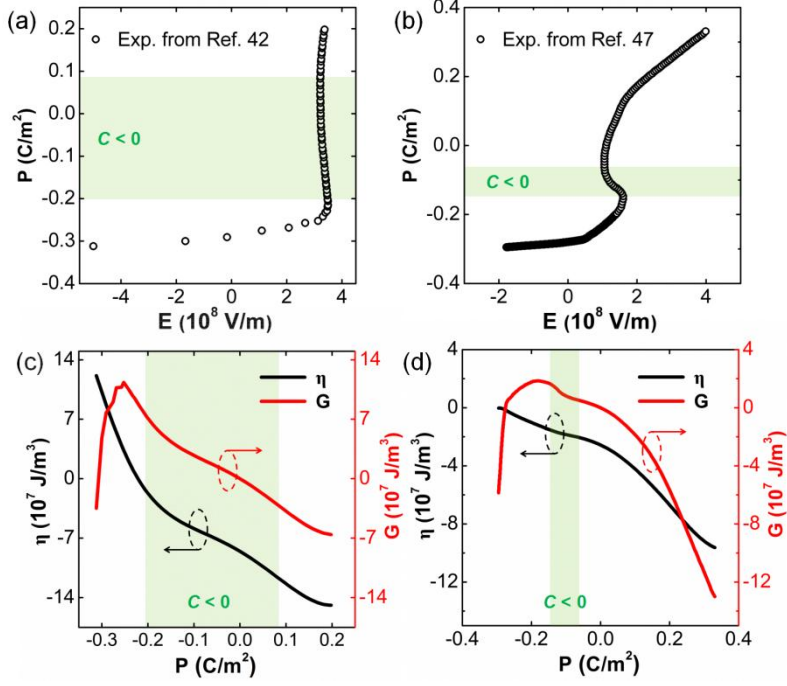


Figure 2. (a,b) The experimental P - E curves in Refs. 42 and 47. (c,d) The corresponding Gibbs free energy and the new thermal potential η profiles as a function of polarization P . The shadow regions represent the NC regions.

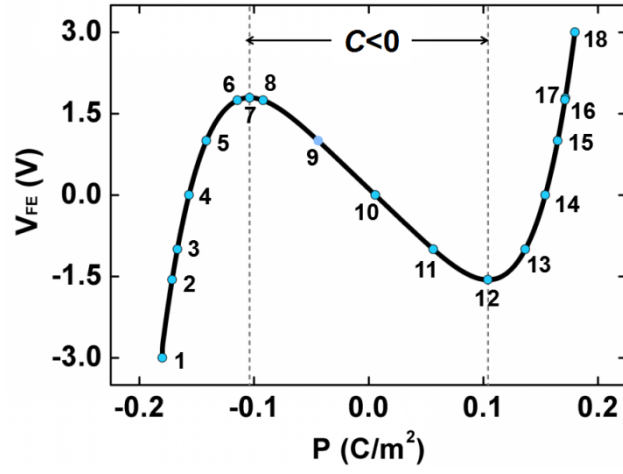


Figure 3. The V_{FE} - P curve of transient NC. Number 1-18 corresponds to different transient polarization states.

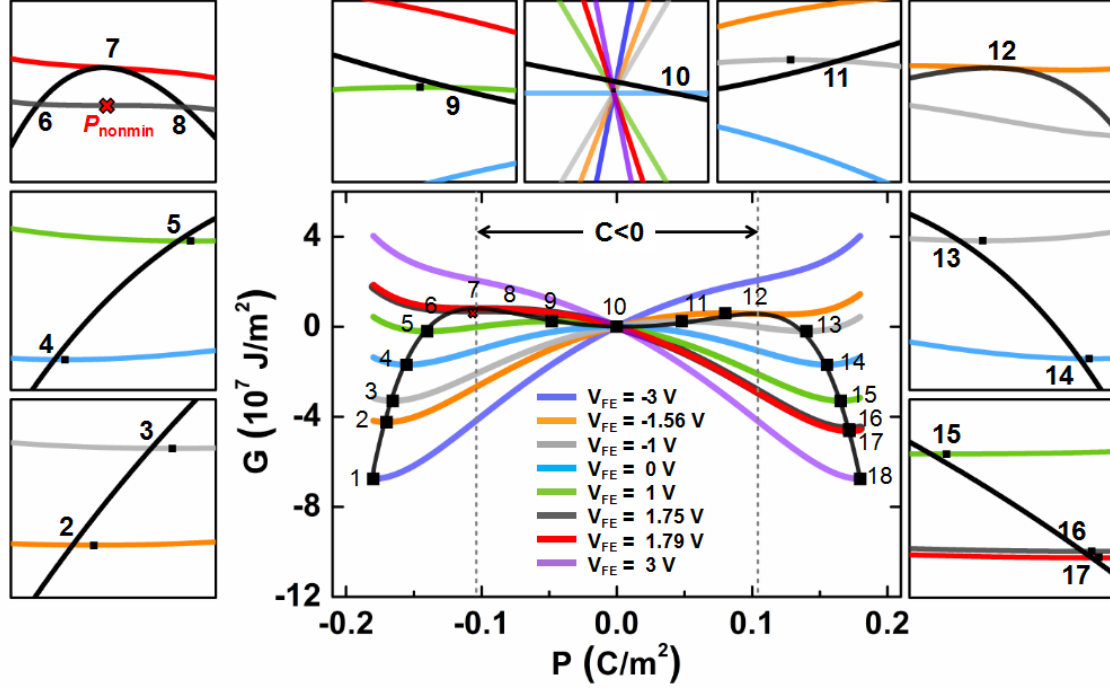


Figure 4. The Gibbs free energy profiles as a function of polarization P at different voltages for the ferroelectric capacitor. Black square dots represent the local extreme points of the Gibbs free energy at different voltages, respectively. The red cross represents the zero derivative point that is not an extreme point. States 1 and 18 are stable and states 2-17 are unstable states. States 1-18 are connected with the black line. The black line expresses the real G in the transient NC process.

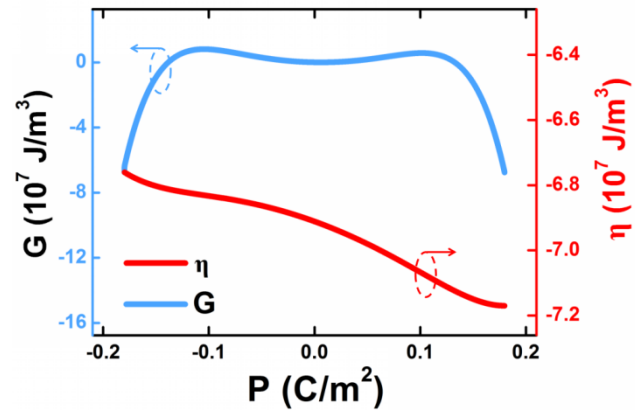


Figure 5. The Gibbs free energy profiles and the new thermal potential η profiles as a function of polarization P .

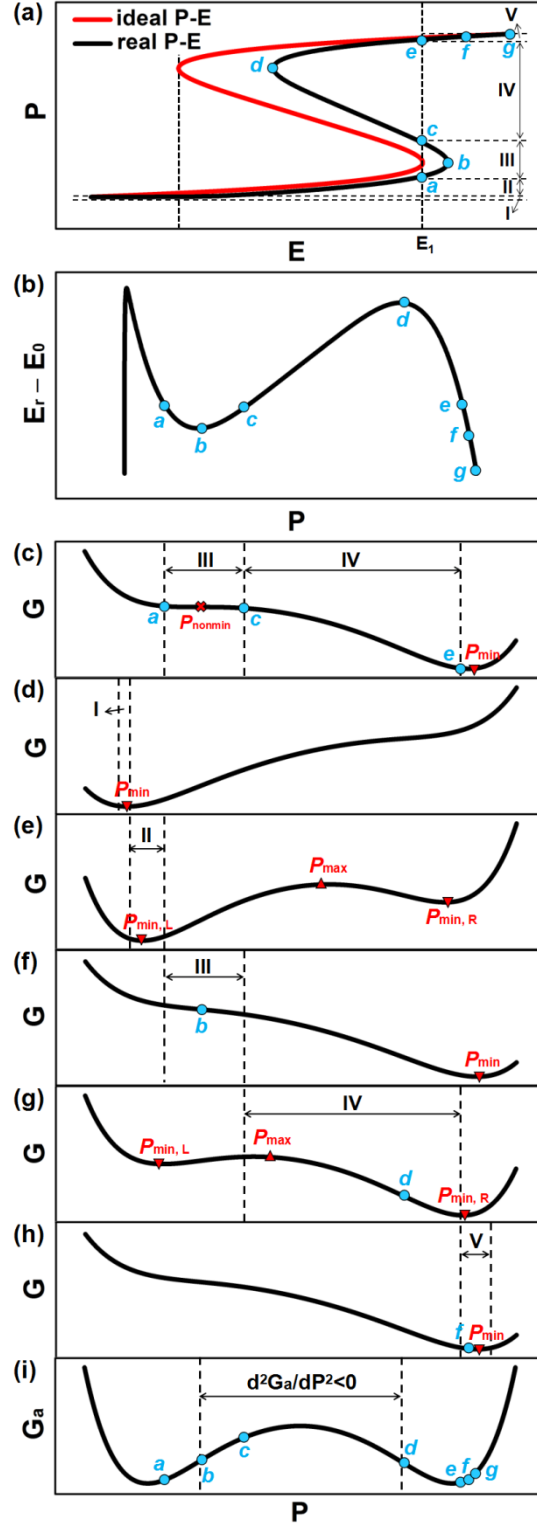


Figure 6. (a) The schematic diagram of ideal P - E curves and real P - E curves. (b) The electric field difference between real P - E curves and ideal P - E curves as a function of polarization P . (c) The Gibbs free energy profile at $E=E_1$. The Gibbs free energy profile for regions I (d), II (e), III (f), IV (g) and V (h). The region III, IV and V correspond to state $a \rightarrow b \rightarrow c$, $c \rightarrow d \rightarrow e$ and $e \rightarrow f \rightarrow g$, respectively. (i) The elastic Gibbs free energy profile as a function of polarization P .

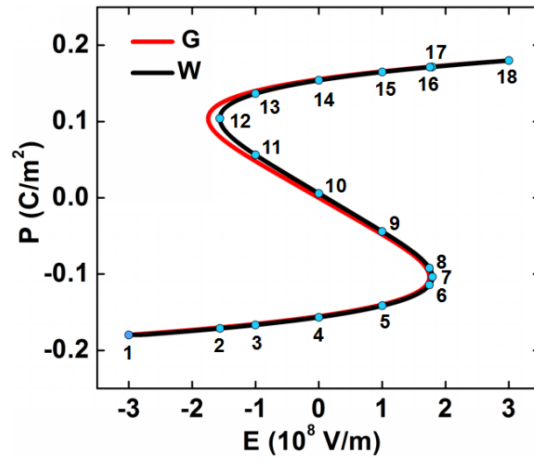


Figure 7. The P - E curves for elastic Gibbs free energy and electrostatic force work. Number 1-18 corresponds to transient polarization states in Figure 3.

Table 1. Simulation parameters for the R -FEC circuit.

Parameter	Quantity	Value ²⁵
α		$-1.05 \times 10^9 \text{ m/F}$
β	Landau expansion coefficient	$10^7 \text{ m}^5/\text{C}^2\text{F}$
γ		$6 \times 10^{11} \text{ m}^9/\text{C}^4\text{F}$
ρ	Viscosity coefficient	500 m sec/F
d_{FE}	Ferroelectric thickness	10 nm
A	Capacitor area	$50^2 \mu\text{m}^2$
R	External resistance	$50 \text{ k}\Omega$